Acta Crystallographica Section D
Biological Crystallography
ISSN 1399-0047

Domain mobility as probed by small-angle X-ray scattering may account for substrate access to the active site of two copper-dependent amine oxidases

Enrico Dainese,[a,b]*‡ Annalaura Sabatucci,[a]‡ Francesca Pintus,[c] Rosaria Medda,[c] Clotilde Beatrice Angelucci,[d] Giovanni Floris[c]*§ and Mauro Maccarrone[b,e]*§

[a]Faculty of Bioscience and Technology for Food Agriculture and Environment, University of Teramo, Teramo, Italy, [b]European Center for Brain Research (CERC)/Santa Lucia Foundation, Rome, Italy, [c]Department of Sciences of Life and Environment, University of Cagliari, Cagliari, Italy, [d]Faculty of Veterinary Medicine, University of Teramo, Teramo, Italy, and [e]Center of Integrated Research, Campus Bio-Medico University of Rome, Rome, Italy

‡ These authors should be considered joint first authors.
§ These authors should be considered equal senior authors.

Correspondence e-mail: edainese@unite.it, gfloris@unica.it, m.maccarrone@unicampus.it

Received 22 October 2013
Accepted 26 May 2014

Amine oxidases are a family of dimeric enzymes that contain one copper(II) ion and one 2,4,5-trihydroxyphenyalanine quinone per subunit. Here, the low-resolution structures of two Cu/TPQ amine oxidases from lentil (*Lens esculenta*) seedlings and from *Euphorbia characias* latex have been determined in solution by small-angle X-ray scattering. The active site of these enzymes is highly buried and requires a conformational change to allow substrate access. The study suggests that the funnel-shaped cavity located between the D3 and D4 domains is narrower within the crystal structure, whereas in solution the D3 domain could undergo movement resulting in a protein conformational change that is likely to lead to easier substrate access.

1. Introduction

Quinoprotein copper-containing amine oxidases (CAOs; EC 1.4.3.22, formerly EC 1.4.3.6) are found in bacteria, yeasts, fungi, plants and mammals, where they catalyse the oxidative deamination of primary amines to the corresponding aldehydes, with the concomitant reduction of molecular oxygen to hydrogen peroxide. In prokaryotes, CAOs allow the utilization of various amine substrates as a source of carbon and nitrogen (Wilce *et al.*, 1997; Wilmot *et al.*, 1997). In eukaryotes, CAOs play a role in cell differentiation and growth, wound healing, detoxification and cell signalling (Kumar *et al.*, 1996).

The ping-pong catalytic mechanism utilized by CAOs can be divided into two steps. The 'reductive half-reaction' involves the oxidation of an amine to the corresponding aldehyde and the formation of a reduced form of the 6-hydroxydopa (2,4,5-trihydroxyphenethylamine) quinone (TPQ) cofactor: $E_{ox} + R\mathrm{CH_2}\text{–}\mathrm{NH_3^+} \rightarrow E_{red}\text{–}\mathrm{NH_3^+} + R\mathrm{CHO}$. The 'oxidative half-reaction' involves the re-oxidation of the enzyme with concomitant release of ammonium and hydrogen peroxide: $E_{red}\text{–}\mathrm{NH_3^+} + \mathrm{O_2} + \mathrm{H_2O} \rightarrow E_{ox} + \mathrm{NH_4^+} + \mathrm{H_2O_2}$.

CAOs are homodimers and each subunit has a molecular mass of 70–90 kDa and contains an active site with a tightly bound copper(II) ion and a 2,4,5-trihydroxyphenylalanine quinone (TPQ or TOPA; Janes *et al.*, 1990). Several CAOs, including CAO from pea (*Pisum sativum*; PSAO) and from bovine serum, a lysyl oxidase from *Pichia pastoris* and the human vascular adhesion protein-1 (VAP-1), have been crystallized and characterized by single-crystal X-ray diffraction (Guss *et al.*, 2009 and references therein).

Sequence homology is very high in plants (varying from ~90 to 98%), but is low when plant enzymes are compared with those found in animals and bacteria. However, CAOs have remarkably conserved structures, with mushroom-like architectures made up of three or four topological domains (Guss *et al.*, 2009).

The active site is situated in the large D4 domain consisting of a β-sandwich of 18 strands in two twisted antiparallel sheets. The two smaller D2 and D3 domains have the same α–β fold. The N-terminal D1 domain, the biological function of which remains unknown, constitutes the stalk of the mushroom shape in prokaryotic CAOs but is not present in mammalian and plant CAOs (Kumar *et al.*, 1996).

The well defined active site of CAOs is buried, and substrate access to it apparently requires a substantial rearrangement of the polypeptide fold (Kumar *et al.*, 1996). This active site shows the following structural and functional peculiarities. (i) TPQ is derived from the Cu-catalysed oxidation of a post-translationally modified tyrosine residue in the consensus sequence Asn-Tyr-Asp/Glu of the polypeptide chain (Mu *et al.*, 1992). (ii) The copper(II) ion is coordinated by the imidazole groups of three conserved histidine residues and by two water molecules (equatorial We and axial Wa). (iii) TPQ is close but not bound to copper(II) and apparently has high rotational mobility. (iv) After amine nucleophilic attack, proton abstraction requires the presence of a base, which has been identified as a conserved aspartate residue. (v) A tyrosine residue seems to play an important role in the active site owing to a hydrogen bond that it makes to O4 of TPQ.

Although a lysine residue (Lys296) has been suggested to be present in the active site of PSAO crystals, where it forms a hydrogen bond to the phenolic group of TPQ (Kumar *et al.*, 1996; Duff *et al.*, 2004) demonstrated that the published crystal structure showed TPQ in a nonproductive so-called 'on-copper' conformation; the role of Lys296 in the 'off-copper' conformation remains controversial. Incidentally, the 'on-copper' and 'off-copper' conformations refer to the orientation of TPQ and copper, as described previously (Dawkes & Phillips, 2001).

In this investigation, the solution structures of two different CAOs (from lentil seedlings and from *Euphorbia* latex) have been reconstructed from SAXS data, showing that they share the same topology and closely resemble the crystal structure of PSAO. Experimental evidence strongly suggests that in solution these homodimers have specific regions that could undergo conformational change; in particular, the D3 domain seems to move with respect to the rest of the protein, thus increasing the accessibility of the active site.

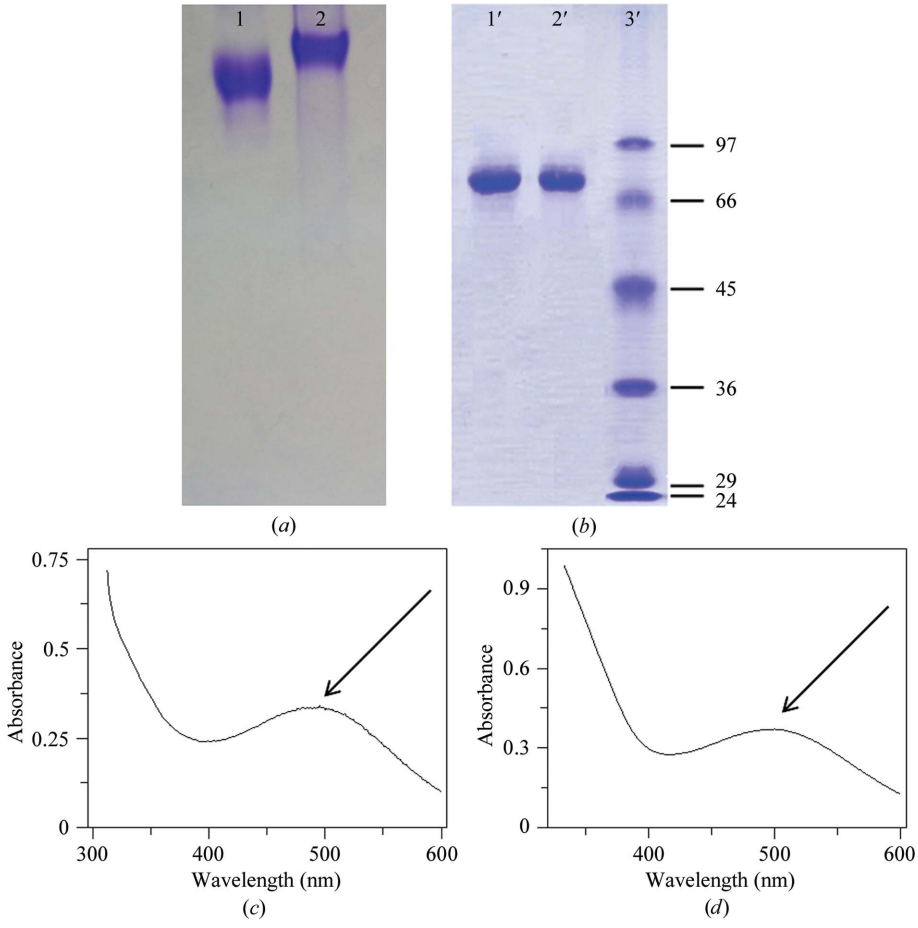

Figure 1
(*a*) PAGE under nondenaturing conditions and (*b*) SDS–PAGE in the presence of β-mercaptoethanol of purified LSAO (lanes 1 and 1′) and ELAO (lanes 2 and 2′) exclude any polydispersity of the samples. Lane 3′ contains molecular-mass marker (labelled in kDa). Visible absorption spectra of ELAO (56 μM) and LSAO (91 μM) are shown in (*c*) and (*d*), respectively. The oxidized forms of CAOs show a distinct pink colour, with peaks in the visible region at 498 nm (LSAO) and 496 nm (ELAO) (marked with arrows). The shape of the peaks and the absence of shoulders in these peaks clearly indicate a fully functional enzyme.

2. Materials and methods

2.1. Reagents and enzyme purification

All reagents were of the highest analytical grade. 1,4-Diaminobutane dihydrochloride (putrescine) and 1,5-diaminopentane dihydrochloride (cadaverine) were purchased from Sigma–Aldrich (St Louis, Missouri, USA). Amine oxidase from lentil (*Lens esculenta*) seedlings was prepared as reported by Floris *et al.* (1983), whereas that from *E. characias* latex was purified as described by Padiglia *et al.* (1998). The purified enzymes were exhaustively dialyzed against 25 mM potassium phosphate buffer pH 7.0, concentrated by ultrafiltration and centrifuged at 14 300g for 30 min. The pellet was discarded. The protein concentration in the supernatant was measured by the Bradford method using bovine serum albumin to generate calibration curves (Bradford, 1976). Only proteins of the highest quality were utilized on the basis of a TPQ:dimer ratio of 1.9:2.1. The concentration of the quinone was determined by titration with the carbonyl reagent PHY, giving a hydrazone with a very high extinction coefficient at 445 nm (ε_{445} = 6.4 × 10^4 M^{-1} cm^{-1}; Medda *et al.*, 1995).

Table 1
Data-collection and scattering-derived parameters.

	LSAO	ELAO
Data-collection parameters		
Instrument	SWING (SOLEIL synchrotron)	
Wavelength (Å)	1.033	
q range (Å^{-1})	0.01–0.60	
Exposure time (s)	25	
Concentration (mg ml^{-1})	2.0	
Temperature (°C)	10	
Structural parameters		
$I(0)$ (cm^{-1}) [from $P(r)$]	0.32	0.32
R_g (Å) [from $P(r)$]	37.25 ± 0.03	35.83 ± 0.05
$I(0)$ (cm^{-1}) (from Guinier)	0.32	0.32
R_g (Å) (from Guinier)	36.8 ± 0.1	35.5 ± 0.1
D_{max} (Å)	120	120
Porod volume estimate (Å^3)	282090	235860
Dry volume calculated from sequence (Å^3)	178000	178000
Partial specific volume (cm^3 g^{-1})	0.73	0.73
Contrast (10^{10} cm^{-2})	3.047	3.047
Molecular mass from $I(0)$ (kDa)	200	200
Monomer molecular mass from sequence (kDa)	73.5	74.0
Software employed		
Primary data reduction	*FOXTROT*	
Data processing	*FOXTROT*, *PRIMUS*, *KALEIDAGRAPH*	
Ab initio analysis	*DAMMIN*	
Validation and averaging	*DAMAVER*	
Rigid-body modelling	*SASREF*	
Computation of model intensities	*CRYSOL*	
Three-dimensional graphical representations	*Discovery Studio Visualizer* 3.0, *Swiss-PdbViewer*	

For SAXS measurements, the samples were appropriately diluted by determining the concentrations from absorption spectra using an ε_{498} of 4100 M^{-1} cm^{-1} for lentil seedling amine oxidase (LSAO) and an ε_{496} of 6000 M^{-1} cm^{-1} for *E. characias* amine oxidase (ELAO) (Floris *et al.*, 1983; Padiglia *et al.*, 1998).

The monodispersity of the protein dimers was verified by size-exclusion HPLC chromatography performed on a PE Series 200 System (Perkin Elmer Life and Analytical Sciences, Boston, Massachusetts, USA) using a Yarra SEC-4000 column (Phenomenex Inc.) and allowed the presence of higher aggregation states to be ruled out.

2.2. Polyacrylamide gel electrophoresis (PAGE)

Electrophoresis under nondenaturing conditions was performed as described previously (Gabriel, 1971). The protein band with AO activity was detected after the electrophoretic run by staining the gel in 100 mM potassium phosphate buffer pH 7.0 containing 100 µg peroxidase, 1 mg benzidine and 1 mM putrescine.

SDS–PAGE was carried out according to Weber & Osborn (1969). The protein samples for SDS–PAGE were heated at 100°C for 5 min in 10 mM Tris–HCl buffer pH 7.0 containing 1% SDS and 100 mM β-mercaptoethanol. For SDS–PAGE analysis the following molecular-weight standards were used: phosphorylase b (97 kDa), bovine serum albumin (66 kDa), ovalbumin (45 kDa), glyceraldehyde-3-phosphate dehydrogenase (36 kDa), carbonic anhydrase (29 kDa) and trypsinogen (24 kDa).

2.3. Spectroscopic analysis and enzyme assay

The UV–visible absorption spectra of the CAOs were recorded at 25°C using an Ultrospec 2100 spectrophotometer (Biochrom Ltd, Cambridge, England).

The CAO enzymatic activity was measured as previously reported (Floris *et al.*, 1983). Oxygen uptake was determined with a Clark-type electrode coupled to a OXYG1 Hansatech oxygraph (Hansatech Instruments Ltd, King's Lynn, England). The temperature of the reaction chamber was kept at 37°C using a circulating water bath. The solution (1 ml) containing the enzyme was maintained for 10 min with constant stirring and the reaction was started by the addition of the substrate (putrescine).

2.4. SAXS analysis

SAXS measurements were carried out on the SWING beamline at the SOLEIL synchrotron-radiation facility, Saint-Aubin, France. The two-dimensional detector was set up at a distance of 1806.9 mm from the sample holder, allowing the scattering intensity to be recorded in a momentum-transfer range of 0.01 Å^{-1} $\leq q \leq$ 0.60 Å^{-1} [$q = (4\pi/\lambda)\sin\theta$, where 2θ is the scattering angle and λ is the wavelength of the monochromatic beam). The sample holder was a quartz capillary kept under vacuum at a temperature of 10°C. Absolute calibration of the beam was performed according to standard procedures using water as a primary standard (Mylonas & Svergun, 2007).

The proteins (LSAO and ELAO) were analyzed in the same buffer as used for purification (25 mM potassium phosphate pH 7.0). 5 mM DTT was added to the solution in order to prevent radiation-damage effects. Each sample was measured at three different concentrations: 0.5, 1.0 and 2.0 mg ml^{-1}. As shown in Supplementary Fig. S1[1], no aggregation or interparticle effects were observed in the curves of both proteins. Thus, data analyses were performed using protein samples at 2.0 mg ml^{-1}. For each acquisition, a total volume of 50 µl solution was fluxed into the capillary and, after inspecting for radiation damage, 25 frames (1 s each) were recorded and averaged. Buffer signal was successively subtracted. All of these steps were performed with the *FOXTROT* program available at the SWING beamline workstation.

Data treatment was performed with *PRIMUS* (Konarev *et al.*, 2003), which contains different modules, including *GNOM* (Svergun, 1992). The latter program allows the $p(r)$ function to be obtained, calculation of the radius of gyration in real space and estimation of the maximum dimension of the particle (D_{max}).

The *ab initio* structures of the proteins were obtained as dummy-atom (DAM) models (Svergun, 1999; Svergun *et al.*, 2001; Volkov & Svergun, 2003) from the regularized curves obtained from *GNOM* as follows. For each structure, ten

[1] Supporting information has been deposited in the IUCr electronic archive (Reference: TZ5047).

independent *DAMMIN* models were generated, averaged (*DAMAVER*) and filtered (*DAMFILT*) to obtain a final model representative of the protein envelopes.

The theoretical scattering curves from the crystal structures were calculated with *CRYSOL* (Svergun *et al.*, 1995) and fitted against the experimental curves.

The movement simulation and modelling against solution scattering data for the D3 domain was performed with *SASREF* (Petoukhov & Svergun, 2005). At least three independent refinements were conducted without observing any spread of conformational space of the resulting models.

Three-dimensional structural images were built with *Discovery Studio Visualizer* 3.0 (Accelrys Software Inc.) and *Swiss-PdbViewer* (http://www.expasy.org/spdbv/; Guex & Peitsch, 1997). Low/high-resolution structure superpositions and NSD calculations were performed with *SUPCOMB* 2.0 (Kozin & Svergun, 2001).

2.5. Sequence analysis and homology modelling

Sequence alignments were performed with *Clustal Omega* as available at http://www.uniprot.org (The UniProt Consortium, 2012).

Three-dimensional model structures of LSAO and ELAO were retrieved from the SWISS-MODEL Repository automated homology modelling database (Arnold *et al.*, 2006; Kiefer *et al.*, 2009; Kopp & Schwede, 2004). For both the LSAO sequence (UniProtKB ID P49252) and the ELAO precursor sequence (UniProtKB ID Q9SW90) the server identified the crystal structure of PSAO subunit *B* (PDB entry

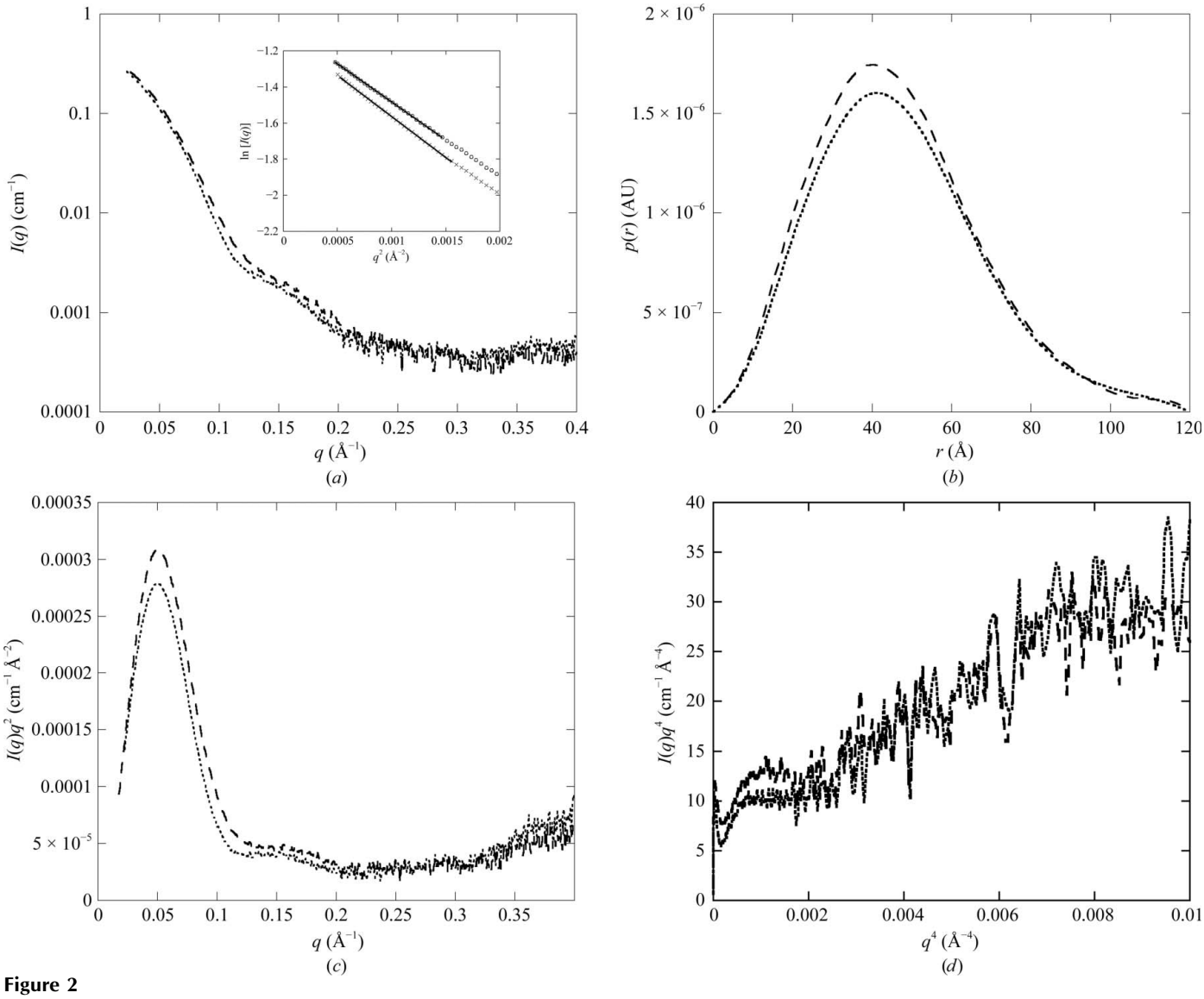

Figure 2
The scattering patterns (*a*) of LSAO (dotted line) and ELAO (dashed line) are rather superimposable on each other. From the Guinier region (inset), radii of gyration of 36.8 ± 0.1 Å for LSAO (crosses) and 35.5 ± 0.1 Å for ELAO (open circles) were calculated. From the $I(0)/c$ value, a molecular mass of ∼200 kDa was calculated for both enzymes. The $p(r)$ functions (*b*) of the two proteins have similar shapes and are characterized by the same maximum dimension (D_{max}) of the particle (120 Å). The Kratky (*c*) and Porod (*d*) plots indicate that both proteins are globular and suggest the presence of a more movable region (see text for further details).

1ksi, chain *B*; Kumar *et al.*, 1996) as a template from a *BLAST* (Altschul *et al.*, 1990) search. The resulting sequence identity with the template was 92% for LSAO and 90% for ELAO. As the sequence identity was higher than 50%, the models were calculated by the server in automated mode (model-quality assessment was performed *via ANOLEA* and *GROMOS*).

3. Results

3.1. Enzyme purification and activity assay

Purified LSAO and ELAO were tested for homogeneity and monodispersity by PAGE. Only one protein band with enzymatic activity was detected by PAGE either under non-denaturing conditions or by SDS–PAGE in the presence of β-mercaptoethanol (Figs. 1*a* and 1*b*), confirming the absence of any polydispersity (*i.e.* aggregation) of the analysed protein samples. The purified AOs showed a k_c using putrescine as substrate that was typical of highly purified enzymes (LSAO, k_c = 155 s^{-1}; ELAO, k_c = 23 s^{-1}).

3.2. Spectroscopic features

Owing to the presence of TPQ, the oxidized forms of CAOs show a distinctive pink colour with peaks in the visible region at 498 nm for LSAO (ε_{498} = 4100 M^{-1} cm^{-1}) and at 496 nm for ELAO (ε_{496} = 6000 M^{-1} cm^{-1}) (Figs. 1*c* and 1*d*). Any difference in the enzyme structures can be attributed to these regions of the spectra. In Fig. 1, the absence of shoulders in these peaks for both LSAO and ELAO is an unambiguous indication of a purified and fully functional enzyme (Medda *et al.*, 1995).

3.3. Structural parameters of LSAO and ELAO

Data collection and scattering-derived parameters for the analysed LSAO and ELAO samples are reported in Table 1, according to the publication guidelines recently suggested by Jacques *et al.* (2012).

The scattering patterns of LSAO and ELAO are very similar, as shown in Fig. 2(*a*). Analysis of the Guinier region (inset in Fig. 2*a*) gave radii of gyration of 36.8 ± 0.1 Å for LSAO and 35.5 ± 0.1 Å for ELAO. A molecular mass of ∼200 kDa was calculated from $I(0)/c$ for both proteins; this value is 2.72 and 2.70 times higher with respect to those calculated for the amino-acid sequences of the LSAO and ELAO monomers, respectively. These values appear to be quite acceptable for a dimeric protein. However, molecular-mass estimation from $I(0)/c$ is never very accurate because it is affected by several physicochemical parameters, including the determination of the partial specific volume of the protein, the solvent electron density, the contribution of the shell of hydration of the protein to the overall scattering and the exact determination of the protein concentration (Mylonas & Svergun, 2007); last but not least, it is affected by protein flexibility.

Both proteins show very similar $p(r)$ functions with a bell-like shaped curve and the same value for the maximum diameter (D_{max} = 120 Å) as estimated

```
VTPLHVQHPLDPLTKEEFLA--VQTIVQNKYPISN-NRLAFHYIGLDDPEKDHVLRYETH   57  Q43077 PSAO
FTPLHTQHPLDPITKEEFLA--VQTIVQNKYPISN-NKLAFHYIGVDDPEKDLVLKYETS   57  P49252 LSAO
VTPLHTQHPLDPLTKEEFLAHIVQTIVQNKYPISNNNKLAFHYIGVDDPEKDLVLKYETS   60  Q9SW90 ELAO
.****.******:*******  ************* *:*******:****** **:***

PTLVSIPRKIFVVAIINSQTHEILINLRIRSIVSDNIHNGYGFPILSVD-----EQSL-A  111  Q43077 PSAO
PTLISIPRKIFVVAIINSQTHEILIDLTIKSIVSDNIHNGYGFPVLSAA-----EQFL-A  111  P49252 LSAO
PTLISIPRKIFVVAIITRSQTEILIDLTRS----VSDNNGHGFPVLSAAIIRRHEQFLAI  116  Q9SW90 ELAO
***:************. .  ****:*        . .**:***:**.      ** *

IKLPLKYPPFIDSVKKRGLNLSEIVCSSFTMGWFGEEKNVRTVRLDCFMKESTVNIYVRP  171  Q43077 PSAO
IDLPLKYPPFIASVNKRGLNISEIVCSSFTMGWFGEEKNSRTVRVDCFMKESTVNIYVRP  171  P49252 LSAO
DELPLKYPPFIASVNKRGLNISEIVCSSFTMGWFGEEKNSRTVRVDFFMKENTVNIYVRP  176  Q9SW90 ELAO
 .********* **:*****:****************** ****:* ****.********

ITGITIVADLDLMKIVEYHDRDIEAVPTAENTEYQVSKQSPPFGPKQHSLTSHQPQGPGF  231  Q43077 PSAO
ITGITIVADLDLMKIVEYHDRDTEAVPTAENTEYQVSKQSPPFGPKQHSLTSHQPQGPGF  231  P49252 LSAO
ITGITIVADLDLMKIVEYHDRGIEAVPTAENTEYQVSKQSPPFGPKQHSLTSHQPQGPGF  236  Q9SW90 ELAO
**********************  ************************************

QINGHSVSWANWKFHIGFDVRAGIVISLASIYDLEKHKSRRVLYKGYISELFVPYQDPTE  291  Q43077 PSAO
QINGTSVSWANWKFHIGFDVRAGIVISLASIYDLEKHKSRRVLYKGYISELFVPYQDPTE  291  P49252 LSAO
QINGTSVSWANWKFHIGFDVRAGIVISLASIYDLEKHKSRRVLYKGYISELFVSYQDPTE  296  Q9SW90 ELAO
**** ********************************************** ******

EFYFKTFFDSGEFGFGLSTVSLIPNRDCPPHAQFIDTYVHSANGTPILLKNAICVFEQYG  351  Q43077 PSAO
EFYFKTFFDSGEFGFGLSTVSLIPNRDCPPHAQFIDTYIHSADGTPIFLENAICVFEQYG  351  P49252 LSAO
EFYFKSYFDSGEFGFGLSYVSLIPNRDCPPHAQFIDTYIHSANGTPIFLENAICVFEQYG  356  Q9SW90 ELAO
*****::*********** ********************:***:****:*:**********

NIMWRHTENGIPNESIEESRTEVNLIVRTIVTVGNYDNVIDWEFKASGSIKPSIALSGIL  411  Q43077 PSAO
NIMWRHTETGIPNESIEESRTEVDLAIRTVVTVGNYDNVLDWEFKTSGWMKPSIALSGIL  411  P49252 LSAO
NIMWRHTETGIPNESIEESRTEVDLIIRTVVTVGNYDNVIDWEFSASGSIKPSIALSGIL  416  Q9SW90 ELAO
********.**************:* :**:*********:****.:** :**********

EIKGTNIKHKDEIKEDLHGKLVSANSIGIYHDHFYIYYLDFDIDGTHNSFEKTSLKTVRI  471  Q43077 PSAO
EIKGTNIKHKDEIKEEIHGKLVSANSIGIYHDHFYIYYLDFDIDGTQNSFEKTSLKTVRI  471  P49252 LSAO
EIKGTNIKHKDEIKEEIHGKLVSADSIGIYHDHFYIYYLDFDIEGTQNSFEKTSLKTVRI  476  Q9SW90 ELAO
***************::*******:******************:**:*************

KDGSSKRKSYWTTETQTAKTESDAKITIGLAPAELVVVNPNIKTAVGNEVGYRLIPAIPA  531  Q43077 PSAO
VDGGSKRKSYWTTETQTAKTESDAKITIGLAPAELVVVNPNIKTAVGNEVGYRLIPAIPA  531  P49252 LSAO
KDGSSKRKSYWTTETQTAKTESDAKITTGLAPRELVVVNPNIKTAVGNEVGYRLIPAIPA  536  Q9SW90 ELAO
 **.*********************** **** ****************************

HPLLTEDDYPQIRGAFTNYNVWVTAYNRTEKWAGGLYVDHSRGDDTLAVWTKQNREIVNK  591  Q43077 PSAO
HPLLTEDDYPQIRGAFTNYNVWVTPYNRTEKWAGGLYVDHSRGDDTLAVWTKKNREIVNK  591  P49252 LSAO
HPLLTEDDYPQIRGAFTNYNVWVTPYNRTEKWAGGLYVDHSRGDDTLAVWTKQNREIVNK  596  Q9SW90 ELAO
************************ ***************************:*******

DIVMWHVVGIHHVPAQEDFPIMPLLSTSFELRPTNFFERNPVLKTLSPRDVAWPGCSN  649  Q43077 PSAO
DIVMWHVVGIHHVPAQEDFPIMPLLSTSFELRPTNFFERNPVLKTLPPRDFTWPGCSN  649  P49252 LSAO
DIVMWHVVGIHHVPAQEDFPIMLLLST-SELRPTNFFERNPVLKTLSPRDVACPGCSN  653  Q9SW90 ELAO
********************** ****  ***************** ***.: *****
```

Figure 3
Sequence alignment of PSAO, LSAO and ELAO. Yellow, the consensus sequence containing the post-translationally modified Tyr residue (TPQ). Green, the three histidine residues coordinating the Cu^{2+} ion in the active site. Red, the Lys296 residue that is supposed to belong to the active site by forming a hydrogen bond to the phenolic group of TPQ (Kumar *et al.*, 1996).

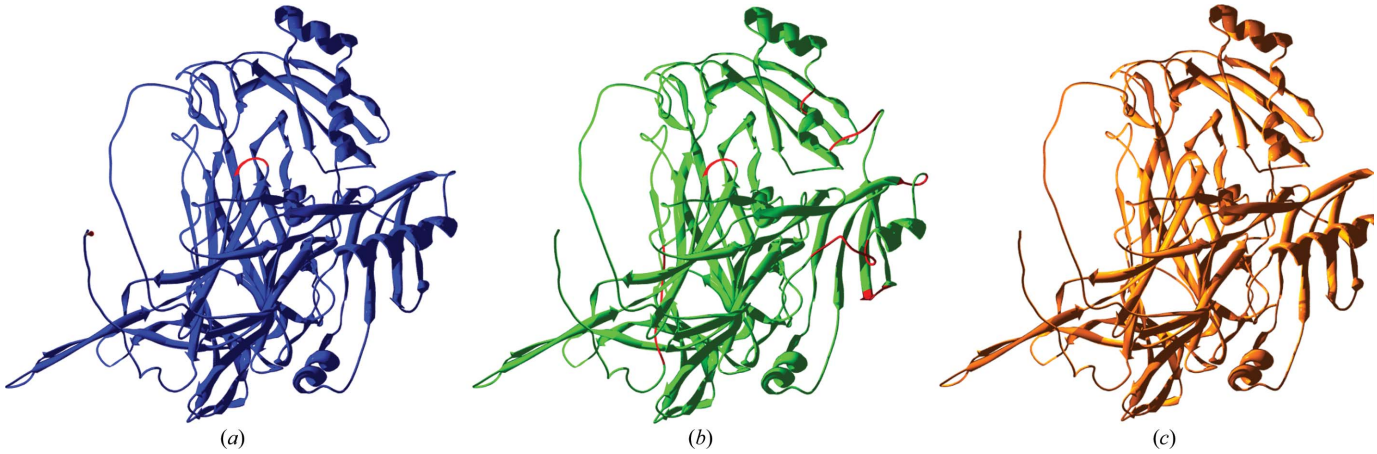

Figure 4
Three-dimensional homology models for (*a*) LSAO (blue) and (*b*) ELAO (green) monomers retrieved from the SWISS-MODEL Repository and compared with the crystal structure of the PSAO 1ksi chain *B* monomer template (*c*) (orange). In the two models, the outlined short red stretches correspond to spatial regions that are non-overlapping with the regions of the template structure.

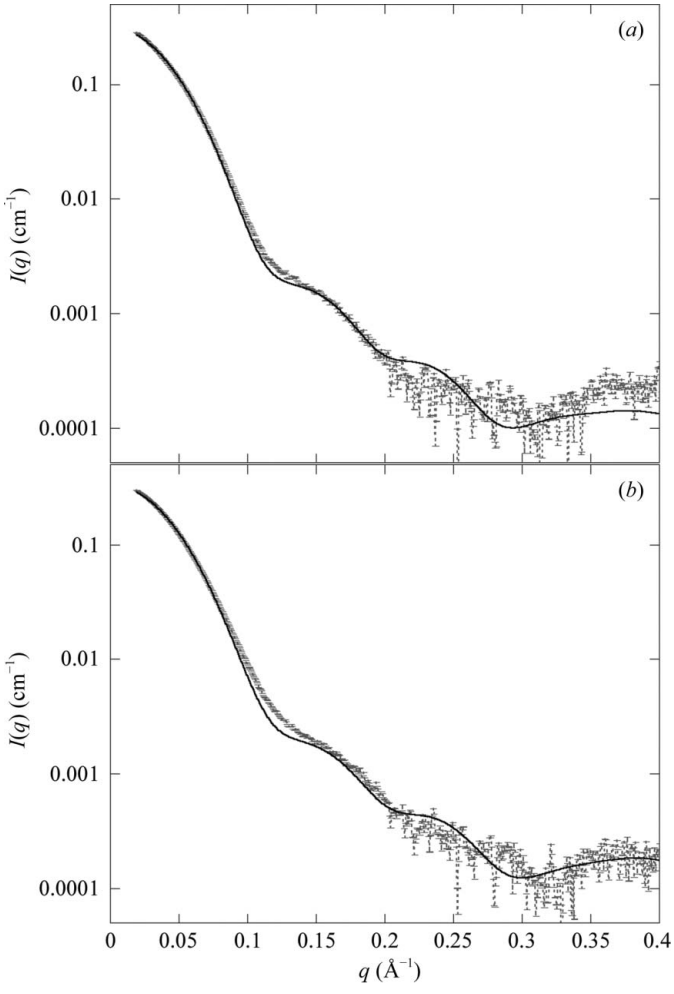

Figure 5
Best fit of the experimental scattering patterns of LSAO (*a*) and ELAO (*b*) to the theoretical pattern calculated from the crystal structure coordinates of PSAO yields quite high χ values (28.5 for LSAO and 29.7 for ELAO). Calculations were made with the *CRYSOL* program as detailed in §2.

with *GNOM* (Svergun, 1992; Fig. 2*b*). The Kratky plots (Fig. 2*c*) for both enzymes clearly show that they have a globular shape. The Porod plots (Fig. 2*d*) seem to confirm this interpretation; in fact, after reaching a plateau at $q^4 < 0.002$ Å^{-4}, the presence of folded protein is clearly indicated; at $q^4 > 0.002$ Å^{-4} the plot instead increases monotonically, suggesting the presence of a more mobile region of the protein (Fig. 2*d*). Interestingly, the Porod volume estimates are 282 090 and 235 860 Å^3 for LSAO and ELAO, respectively, corresponding to molecular masses of ∼166 and 139 kDa, values that are more consistent with dimers than those derived from $I(0)/c$ (Porod volume/1.7 $\simeq$ molecular mass; Fischer *et al.*, 2010).

3.4. Comparison with the available crystal structure

Crystal structures of these two CAOs are not yet available. For both proteins, we have built a three-dimensional structure by homology modelling using the crystal structure of *P. sativum* CAO (PDB entry 1ksi; Kumar *et al.*, 1996) as a template. The sequence alignment (Fig. 3) indicates that the three enzymes share ∼86% sequence identity (569 residues in identical positions; 43 positions with similar residues).

As shown in Fig. 4, the monomeric subunits of both proteins were essentially superimposable on the pea enzyme monomer. For ELAO only seven short regions are not perfectly superposed with the template: Lys39–Val47, Asn59–Asn60, Asp110–Thr112, Ala129–Arg133, Ile140–Glu142, Gly414–Tyr416 and Ser648–Asn654. For LSAO only a short three-residue region (Gly403–Tyr405, corresponding to Gly414–Tyr416 in ELAO) does not fit the crystal structure of PSAO. Notably, the tyrosine residue of the conserved Gly-Asn-Tyr sequence belongs to the TPQ region, but the crystal structure used as the template is in the energetically unlikely 'on-copper' conformation. Therefore, it could be anticipated that the coordinates of the models resulted in slight differences in this region.

Since the monomeric structures of LSAO and ELAO were very similar, in our first analysis step we evaluated the compatibility of the SAXS data (and of the derived low-resolution DAM structures) for both proteins with the crystal structure of the PSAO homodimer.

The experimental curves matched quite nicely with the theoretical curve expected from the crystal structure of PSAO (Fig. 5), although the χ values were somewhat high: 28.5 for LSAO and 29.7 for ELAO, respectively. The most remarkable difference between the theoretical and the experimental scattering patterns resided in the depth of the first minimum for q values around 0.12 Å^{-1}.

The filtered *ab initio* DAM models for the solution structures of LSAO and ELAO both superimpose quite well on the crystal structure of PSAO (Fig. 6). However, the distances calculated with *SUPCOMB* 2.0 from the high-resolution structure are NSD = 1.613 for LSAO and NSD = 1.461 for ELAO. These values may be indicative of the presence of a conformational change of the protein in solution, as the ten independent calculations of the *DAMMIN* models are very stable (*i.e.* NSD = 0.522 ± 0.009 for LSAO and 0.539 ± 0.009 for ELAO). Furthermore, in Fig. 6 it can be noted that for both proteins the D3 domain (highlighted in red) of each subunit does not perfectly fit into the overall shape of the model.

Since the theoretical curve of the crystal structure of PSAO did not perfectly match the experimental curves of LSAO and ELAO, we built a model of these two proteins using the homology models obtained for the subunits. This was performed by superposing the homology models of LSAO and ELAO monomers onto the two subunits of the dimeric structure of PSAO (PDB entry 1ksi). We then fitted the experimental SAXS curves to the theoretical curves of these models using *CRYSOL*. When using the homology models, the comparison of experimental *versus* theoretical curves (Supplementary Fig. S2), with a χ value of 29.5 for both proteins, indicated that the analysis did not significantly improve with respect to the PSAO crystal structure (for LSAO it even became worse).

3.5. Domain mobility of ELAO and LSAO

As previously mentioned, comparison of the theoretical scattering pattern of the crystal structure of PSAO with the experimental patterns of ELAO and LSAO (Figs. 5*a* and 5*b*) shows that for both proteins the two curves display noticeable differences, beyond any experimental or computing error, most remarkably in the small-angle region and around the first subsidiary minimum and maximum. In particular, the first minimum and maximum of the calculated pattern are much sharper than the experimental minimum and maximum, the minimum is shifted towards smaller q values and the oscillations observed in the q range 0.025–0.035 Å^{-1} are different in the experimental pattern. Taking into account the twofold symmetry of the molecule, the experimentally observed weaker modulation suggests that in solution there is some departure from the symmetry observed in the crystal structure. In the same direction, the shapes of the Kratky and Porod plots (Figs. 2*c* and 2*d*) also do not rule out the presence of a region exploring a certain conformational space, in particular through rigid-body movement of a domain around flexible linkers.

Moreover, for both proteins under study it can be noted that the α-helices belonging to the D3 domain of the crystal structure do not overlap with a high electron-density region of the DAM models (Fig. 6).

Thus, we ascertained whether a slight domain movement was allowed in the structures in solution using *SASREF* (see §2). We performed a positional refinement of the D3 domains (residues 106–204) with respect to the D2 (residues 6–96) and D4 (residues 205–676) domains in the 1ksi crystal structure in order to find the best fit against the experimental scattering patterns of LSAO and ELAO in solution. In order to ensure a small conformational change, a contact condition file has been introduced, with the limitation that in both monomers the distance between the C-terminal residue (Val105) of the D2 domain and the N-terminal amino acid (Asp106) of the D3 domain did not exceed 7 Å.

Such a constraint takes into account that the D2 and D3 domains are linked by a relatively short loop consisting of ten

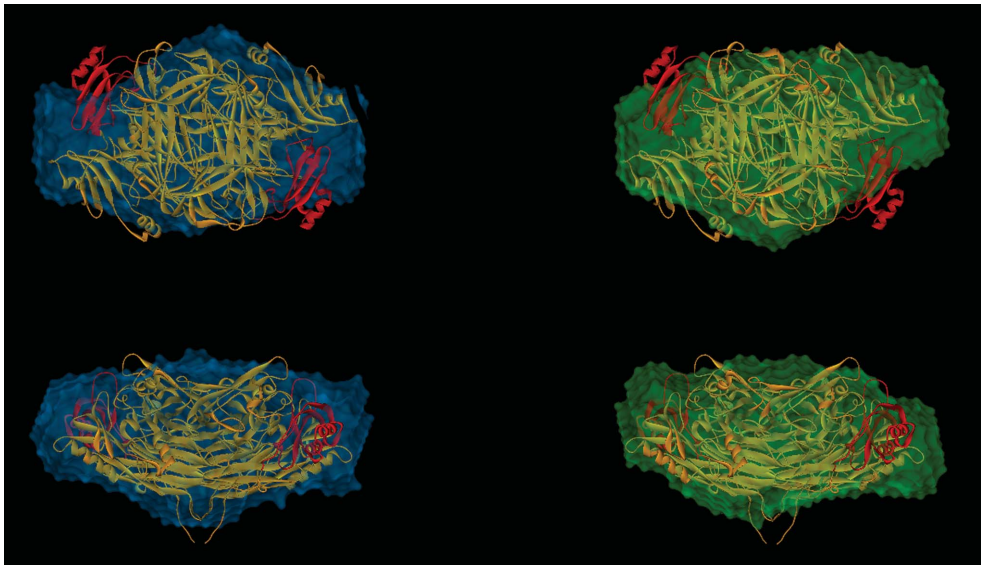

Figure 6
Two different orthogonal projections of the DAM models of LSAO (left) and ELAO (right) superposed on the crystal structure of dimeric PSAO. In the crystal structure, the D2 and D4 domains are shown in orange and the D3 domain is shown in red.

Table 2
Fitting parameters of the crystal structure of PSAO before and after D3 domain movement against experimental data.

	χ value†		NSD‡	
	ELAO	LSAO	ELAO	LSAO
1ksi	29.7	28.5	1.461	1.613
1ksi after D3 domain movement	6.1	12.2	0.913	0.93

† Calculated from scattering curves with *CRYSOL*. ‡ Calculated with *SUPCOMB* between low-resolution DAM models and high-resolution crystal structures.

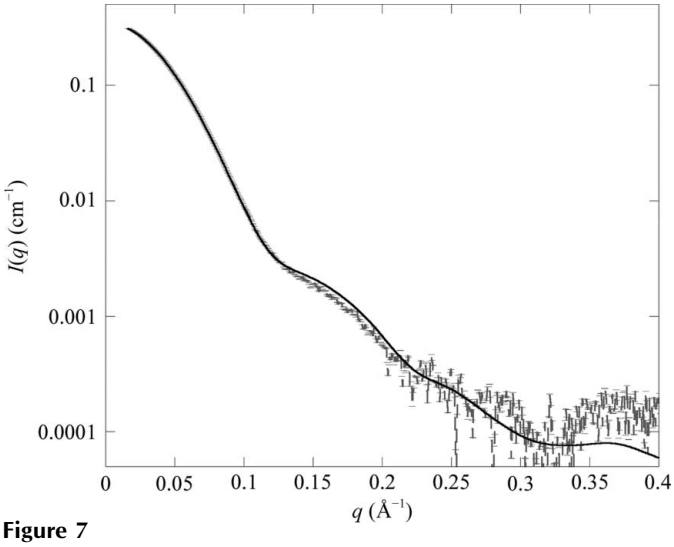

Figure 7
Superposition of the experimental scattering pattern of ELAO (grey) on the theoretical pattern (black) obtained after positional refinement of the D3 domain on the crystal structure 1ksi. Domain movement has been obtained as a roto-translation of the D3 domain with a maximum 5 Å distance constraint between amino acids 105 and 106. The χ value of the fitting is 6.02.

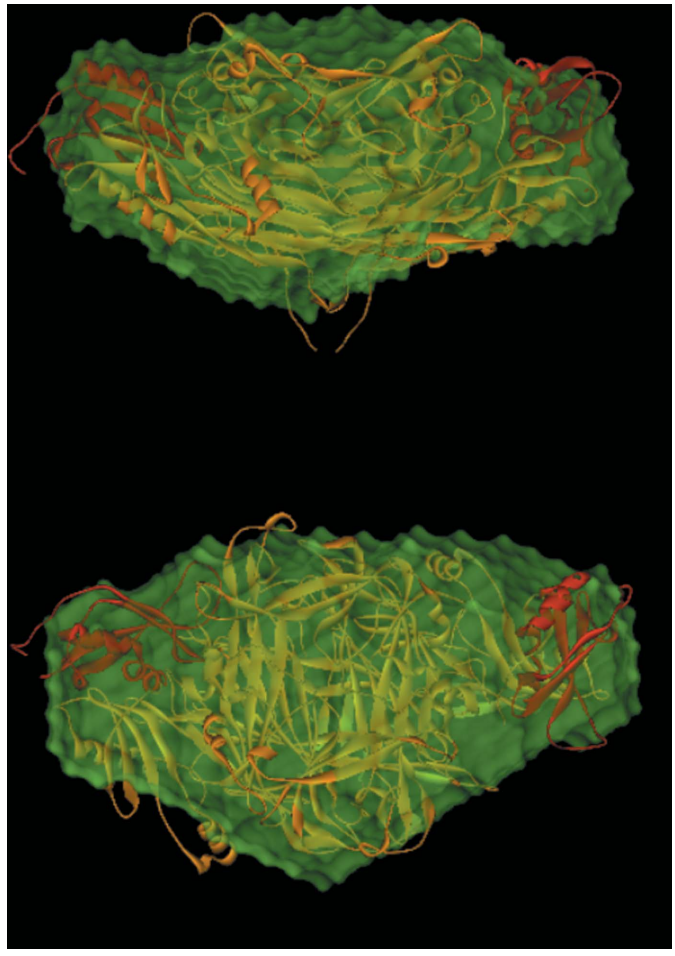

Figure 8
The crystal structure of PSAO (orange) after positional refinement of the D3 domain (red) with *SASREF* strongly indicates that D3 domain movement is occurring in solution.

residues (Asn96–Val105). On the other hand, the D3 and D4 domains are linked by a long region (spanning Asp193–Phe231), where the only structural motif present is the so-called 'loop X' consisting of three residues (Thr222, Ser223 and His224; Kumar *et al.*, 1996). In the PSAO crystal structure, loop X interacts in an antiparallel manner with the corresponding loop of the other subunit. Thus, we performed a positional refinement of the D3 domain taking into account that this region could undergo a large movement without substantially altering the overall conformation of the protein. The resulting structures were found to fit the experimental scattering patterns of LSAO and ELAO in solution much better (see Table 2), implying, in the case of ELAO, an 80% improvement of the quality of the fit with respect to the original coordinates (see Table 2 and Fig. 7). Moreover, the structures obtained by the D3 positional refinement superposed better on the DAM models (see Table 2), as shown in Fig. 8 for ELAO. Thus, the movement of the D3 domain yielded a significant fitting improvement of the SAXS scattering pattern for the proteins in solution. However, we have to take into account that the resolution of the SAXS data and the data treatment only allow it to be concluded that the proteins are not tightly packed as in the crystal structure and, incidentally, the models are compatible with an average solution conformation in which D3 domains can move.

4. Discussion

In this study, we demonstrate that the experimental SAXS patterns of ELAO and LSAO show clear differences compared with the theoretical scattering pattern of the crystal structure of PSAO.

This discrepancy could not be ascribed to aberrations owing to the polydispersity of the two protein samples, as these were checked for purity and monodispersity by native PAGE and SDS–PAGE (Fig. 1) and by size-exclusion HPLC chromatography (data not shown). Moreover, the stability of the Guinier region at three different sample concentrations (see Supplementary Fig. S1) supported the absence of aggregation and/or interparticle interactions. In this context, the importance of excluding any polydispersity in the assessment of the reliability of *ab initio* models should be noted (Dainese *et al.*, 2005; Putnam *et al.*, 2007; Hammel, 2012).

For both ELAO and LSAO, the molecular envelopes of the *ab initio* models show an overall conformation that is slightly

different from that of the crystal structure. In particular, the molecular envelopes suggest that the regions corresponding to the D3 domains are more movable or could change conformation in solution in comparison to the crystal structure (Fig. 6). The observed structural differences could not be ascribed to the *ab initio* modelling procedure. Indeed, as previously demonstrated by others (Meirelles *et al.*, 2011; Trindade *et al.*, 2009), in the analysis of *ab initio* models from a single SAXS curve of a multidomain protein the results obtained using different programs, such as *GASBOR* (Svergun *et al.*, 2001) or *BUNCH* (Petoukhov & Svergun, 2005), lead to similar envelopes. On the other hand, this is not quite unexpected because these models are not sensitive to the flexibility of the parts of the protein after the averaging with the *DAMAVER* suite. Thus, the averaged model from *BUNCH* models looks like a *GASBOR* or *DAMMIN* model.

Differences between the crystal structure and the conformation in solution of multi-domain proteins have previously been reported and have been attributed to the effect of packing forces in the crystal (Grossmann *et al.*, 1992; Vachette *et al.*, 2002).

The first crystal structures of copper amine oxidases from *Escherichia coli* (ECAO; Parsons *et al.*, 1995) and PSAO (Kumar *et al.*, 1996) failed to reveal an accessible portal for the entry of amine substrates into the active site. This led to the initial hypothesis that large domain movements would be required to allow the entry of substrates into and exit of products from the active sites (Kumar *et al.*, 1996; Parsons *et al.*, 1995). The high-resolution structures of other AOs clearly revealed that TPQ is located at the bottom of a funnel-shaped cavity between domains D3 and D4. The opening of the cavity of one subunit is partially hindered by the end of one hairpin from the other subunit, again suggesting some sort of communication between the two active sites.

Here, we demonstrate that a roto-translation of the D3 domain strongly improves the fitting of the SAXS data, suggesting that this region in both the ELAO and LSAO enzymes could undergo remarkable movement without substantially altering the overall structure of the protein. Thus, our data indicate that owing to the presence of crystal-packing forces that lead to a tighter domain interaction, the funnel-shaped cavity located between the D3 and D4 domains could be narrower within the crystal structure. The D3 domain could have a higher mobility in solution, leading to a more accessible portal for substrate entry.

It must be noticed that the X-ray structures of AOs from plants clearly show that the D3 domain is connected to the larger D4 domain through a long partially disordered region of the protein. Thus, the end of the D3 domain and the beginning of the D4 domain are about 50 Å apart. Such a flexible stretch runs over the protein surface and could be responsible for the conformational change that leads to the opening of the funnel-shaped cavity (Fig. 9). The X-ray structure of the human VAP-1 enzyme obtained from two independent studies (Airenne *et al.*, 2005; Jakobsson *et al.*, 2005) clearly confirmed the presence of a structural topology

(*a*)

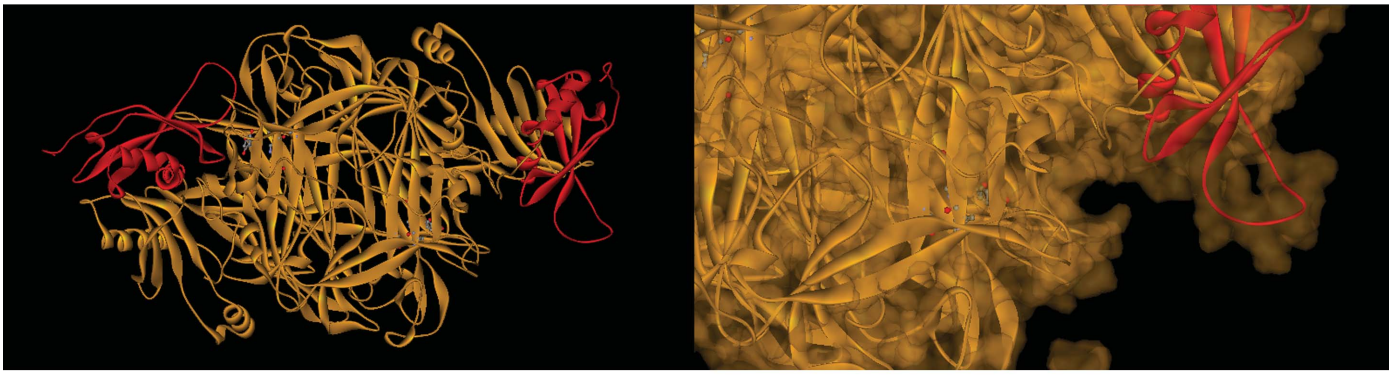

(*b*)

Figure 9
The crystal structure of PSAO after positional refinement of the D3 domain (*b*) shows the active-site residues (ball-and-stick representation) more exposed to the solvent, while in the original crystal structure (*a*) these residues are buried and not accessible.

similar to that of other AOs, made up of domains D2, D3 and D4 assembled in a heart-shaped dimer. In both structures, the D3 domain shares the same conserved core as the D2 domain, but has one additional β-strand and two additional α-helices. Interestingly, in the human VAP-1 enzyme the linker between the D3 domain and the larger D4 domain also consists of a long flexible region (residues 284–322) as observed in plant enzymes (Airenne *et al.*, 2005, Jakobsson *et al.*, 2005). On the basis of the present results, it is tempting to speculate that, as a general feature, CAOs require a domain movement that opens the gate of the active-site channel for substrate entry and product exit.

We acknowledge SOLEIL for granting access to synchrotron-radiation facilities to ED, and Dr Javier Perez for assistance in using the SWING beamline. Financial support from Ministero dell'Istruzione, dell'Università e della Ricerca (grant PRIN 2010-2011 to MM) is gratefully acknowledged. ED and MM wish to thank the EU for a grant from the Biostruct-X project within the FP VII programme. Finally, we acknowledge the inspiring role of Professor Alessandro Finazzi Agrò, who started this collaboration on copper-containing amine oxidases.

References

Airenne, T. T., Nymalm, Y., Kidron, H., Smith, D. J., Pihlavisto, M., Salmi, M., Jalkanen, S., Johnson, M. S. & Salminen, T. A. (2005). *Protein Sci.* **14**, 1964–1974.

Altschul, S. F., Gish, W., Miller, W., Myers, E. W. & Lipman, D. J. (1990). *J. Mol. Biol.* **215**, 403–410.

Arnold, K., Bordoli, L., Kopp, J. & Schwede, T. (2006). *Bioinformatics*, **22**, 195–201.

Bradford, M. M. (1976). *Anal. Biochem.* **72**, 248–254.

Dainese, E., Sabatucci, A., van Zadelhoff, G., Angelucci, C. B., Vachette, P., Veldink, G. A., Finazzi-Agrò, A. & Maccarrone, M. (2005). *J. Mol. Biol.* **349**, 143–152.

Dawkes, H. C. & Phillips, S. E. V. (2001). *Curr. Opin. Struct. Biol.* **11**, 666–673.

Duff, A. P., Trambaiolo, D. M., Cohen, A. E., Ellis, P. J., Juda, G. A., Shepard, E. M., Langley, D. B., Dooley, D. M., Freeman, H. C. & Guss, J. M. (2004). *J. Mol. Biol.* **344**, 599–607.

Fischer, H., de Oliveira Neto, M., Napolitano, H. B., Polikarpov, I. & Craievich, A. F. (2010). *J. Appl. Cryst.* **43**, 101–109.

Floris, G., Giartosio, A. & Rinaldi, A. (1983). *Arch. Biochem. Biophys.* **220**, 623–627.

Gabriel, O. (1971). *Analytical Disc Gel Electrophoresis*, edited by W. B. Jakoby, pp. 565–578. New York: Academic Press.

Grossmann, J. G., Neu, M., Pantos, E., Schwab, F. J., Evans, R. W., Townes-Andrews, E., Lindley, P. F., Appel, H., Thies, W. G. & Hasnain, S. S. (1992). *J. Mol. Biol.* **225**, 811–819.

Guex, N. & Peitsch, M. C. (1997). *Electrophoresis*, **18**, 2714–2723.

Guss, J. M., Zanotti, G. & Salminen, T. A. (2009). *Copper Amine Oxidases*, edited by G. Floris & B. Mondovi, pp. 119–142. Boca Raton: CRC Press.

Hammel, M. (2012). *Eur. Biophys. J.* **41**, 789–799.

Jacques, D. A., Guss, J. M., Svergun, D. I. & Trewhella, J. (2012). *Acta Cryst.* D**68**, 620–626.

Jakobsson, E., Nilsson, J., Ogg, D. & Kleywegt, G. J. (2005). *Acta Cryst.* D**61**, 1550–1562.

Janes, S. M., Mu, D., Wemmer, D., Smith, A. J., Kaur, S., Maltby, D., Burlingame, A. L. & Klinman, J. P. (1990). *Science*, **248**, 981–987.

Kiefer, F., Arnold, K., Künzli, M., Bordoli, L. & Schwede, T. (2009). *Nucleic Acids Res.* **37**, D387–D392.

Konarev, P. V., Volkov, V. V., Sokolova, A. V., Koch, M. H. J. & Svergun, D. I. (2003). *J. Appl. Cryst.* **36**, 1277–1282.

Kopp, J. & Schwede, T. (2004). *Nucleic Acids Res.* **32**, D230–D234.

Kozin, M. B. & Svergun, D. I. (2001). *J. Appl. Cryst.* **34**, 33–41.

Kumar, V., Dooley, D. M., Freeman, H. C., Guss, J. M., Harvey, I., McGuirl, M. A., Wilce, M. C. & Zubak, V. M. (1996). *Structure*, **4**, 943–955.

Medda, R., Padiglia, A., Pedersen, J. Z., Rotilio, G., Finazzi Agrò, A. & Floris, G. (1995). *Biochemistry*, **34**, 16375–16381.

Meirelles, G. V., Silva, J. C., Mendonca, Y. A., Ramos, C. H., Torriani, I. L. & Kobarg, J. (2011). *BMC. Struct. Biol.* **11**, 12.

Mu, D., Janes, S. M., Smith, A. J., Brown, D. E., Dooley, D. M. & Klinman, J. P. (1992). *J. Biol. Chem.* **267**, 7979–7982.

Mylonas, E. & Svergun, D. I. (2007). *J. Appl. Cryst.* **40**, s245–s249.

Padiglia, A., Medda, R., Lorrai, A., Murgia, B., Pedersen, J. Z., Finazzi Agró, A. & Floris, G. (1998). *Plant Physiol.* **117**, 1363–1371.

Parsons, M. R., Convery, M. A., Wilmot, C. M., Yadav, K. D., Blakeley, V., Corner, A. S., Phillips, S. E., McPherson, M. J. & Knowles, P. F. (1995). *Structure*, **3**, 1171–1184.

Petoukhov, M. V. & Svergun, D. I. (2005). *Biophys. J.* **89**, 1237–1250.

Putnam, C. D., Hammel, M., Hura, G. L. & Tainer, J. A. (2007). *Q. Rev. Biophys.* **40**, 191–285.

Svergun, D. I. (1992). *J. Appl. Cryst.* **25**, 495–503.

Svergun, D. I. (1999). *Biophys. J.* **76**, 2879–2886.

Svergun, D. I., Barberato, C. & Koch, M. H. J. (1995). *J. Appl. Cryst.* **28**, 768–773.

Svergun, D. I., Petoukhov, M. V. & Koch, M. H. J. (2001). *Biophys. J.* **80**, 2946–2953.

The UniProt Consortium (2012). *Nucleic Acids Res.* **40**, D71–D75.

Trindade, D. M., Silva, J. C., Navarro, M. S., Torriani, I. C. & Kobarg, J. (2009). *BMC. Struct. Biol.* **9**, 57.

Vachette, P., Dainese, E., Vasyliev, V. B., Di Muro, P., Beltramini, M., Svergun, D. I., De Filippis, V. & Salvato, B. (2002). *J. Biol. Chem.* 277, 40823–40831.

Volkov, V. V. & Svergun, D. I. (2003). *J. Appl. Cryst.* **36**, 860–864.

Weber, K. & Osborn, M. (1969). *J. Biol. Chem.* **244**, 4406–4412.

Wilce, M. C., Dooley, D. M., Freeman, H. C., Guss, J. M., Matsunami, H., McIntire, W. S., Ruggiero, C. E., Tanizawa, K. & Yamaguchi, H. (1997). *Biochemistry*, **36**, 16116–16133.

Wilmot, C. M., Murray, J. M., Alton, G., Parsons, M. R., Convery, M. A., Blakeley, V., Corner, A. S., Palcic, M. M., Knowles, P. F., McPherson, M. J. & Phillips, S. E. (1997). *Biochemistry*, **36**, 1608–1620.